Novel airfoil for improved supersonic aerodynamic performance

Zeyad M. Manaa
Department of Aerospace Engineering, King Fahd University of Petroleum and Minerals (KFUPM), Dhahran, Saudi Arabia, and

Naef A.A. Qasem
Department of Aerospace Engineering, King Fahd University of Petroleum and Minerals (KFUPM), Dhahran, Saudi Arabia and
Interdisciplinary Research Center for Aviation and Space Exploration, King Fahd University of Petroleum and Minerals (KFUPM), Dhahran, Saudi Arabia

International Journal of Numerical Methods for Heat & Fluid Flow

Received 9 June 2024
Revised 30 July 2024
Accepted 5 August 2024

Abstract

Purpose – This study aims to validate the linear flow theory with computational fluid dynamics (CFD) simulations and to propose a novel shape for the airfoil that will improve supersonic aerodynamic performance compared to the National Advisory Committee for Aeronautics (NACA) 64a210 airfoil.

Design/methodology/approach – To design the new airfoil shape, this study uses a convex optimization approach to obtain a global optimal shape for an airfoil. First, modeling is conducted using linear flow theory, and then numerical verification is done by CFD simulations using ANSYS Fluent. The optimization process ensures that the new airfoil maintains the same cross-sectional area and thickness as the NACA 64a210 airfoil. This study found that an efficient way to obtain the ideal airfoil shape is by using linear flow theory, and the numerical simulations supported the assumptions inherent in the linear flow theory.

Findings – This study's findings show notable improvements (from 4% to 200%) in the aerodynamic performance of the airfoil, especially in the supersonic range, which points to the suggested airfoil as a potential option for several fighter aircraft. Under various supersonic conditions, the optimized airfoil exhibits improved lift-over-drag ratios, leading to improved flight performance and lower fuel consumption.

Research limitations/implications – This study was conducted mainly for supersonic flow, whereas the subsonic flow is tested for a Mach number of 0.7. This study would be extended for both subsonic and supersonic flights.

Practical implications – Convex optimization and linear flow theory are combined in this work to create an airfoil that performs better in supersonic conditions than the NACA 64a210. By closely matching the CFD results, the linear flow theory's robustness is confirmed. This means that the initial design phase no longer requires extensive CFD simulations, and the linear flow theory can be used quickly and efficiently to obtain optimal airfoil shapes.

Social implications – The proposed airfoil can be used in different fighter aircraft to enhance performance and reduce fuel consumption. Thus, lower carbon emission is expected.

Originality/value – The unique aspect of this work is how convex optimization and linear flow theory were combined to create an airfoil that performs better in supersonic conditions than the NACA 64a210. Comprehensive CFD simulations were used for validation, highlighting the optimization approach's strength and usefulness in aerospace engineering.

Keywords Airfoil optimization, Supersonic flight, Convex optimization, Aerodynamics performance, Linear flow theory, CFD

Paper type Research paper

The authors thank the support from the Department of Aerospace Engineering, King Fahd University of Petroleum & Minerals (KFUPM), Dhahran, Saudi Arabia.

Declaring conflict of interest: Authors have no conflict of interest to declare.

International Journal of Numerical Methods for Heat & Fluid Flow

0961-5539
DOI 10.1108/HFF-06-2024-0433

Nomenclature

Abbreviations

NACA = National Advisory Committee for Aeronautics;
AOA = angle of attack;
ASO = aerodynamic shape optimization; and
CFD = computational fluid dynamics.

Symbols

$\mathbb{R}^n$ = real numbers vector of degree n;
a_i = airfoil's upper surface polynomial coefficients;
b_i = airfoil's lower surface polynomial coefficients;
c_d = drag coefficient;
c_m = moment coefficient;
g_0 = objective function;
g_i = constraints;
x_c = payload location along the *x*-direction;
y_c = payload location along the *y*-direction;
h = static enthalpy, kJ/kg;
D = drag force, kN;
F = lift coefficient, dimensionless;
L = lift force, kN;
M = Mach number;
i = counter;
n = polynomial degree;
p = static pressure, kPa;
r = payload radius;
y = airfoil's surface parametrization function (polynomial function);
z = camber line; and
$\boldsymbol{Q}$ = positive definite matrix.

Greek letters

Λ_1 = camber line drag;
Λ_2 = thickness drag;
ζ_{max} = airfoil maximum thickness;
α = angle of attack, degree/rad;
λ = convexity tuning parameter;
ρ = density, Kg/m^3; and
$\boldsymbol{v}$ = design parameter vector.

Subscript

l_o = zero left;
l = lower surface (except for $c_l \triangleq$ lift coefficient); and
u = upper surface.

1. Introduction

Airfoil, in general, is any structure that is meant to manipulate the flow of a fluid around it to get a reaction, which, in aerospace applications, is to generate aerodynamic lift. Airfoils not only make heavier-than-air flights possible when used as a wing section but also can be used in other devices

like wind turbines, spoilers and helicopters. The airflow response when disturbed is something natural that is leveraged by the airfoil's shape design to get the desired aerodynamic forces. Airfoil design and jet engines are responsible for driving modern aircraft (Abdulrahman *et al.*, 2023). The history of the development of wing sections is rich. Early in the aerospace community, the development of airfoils was almost totally empirical (Abbott and Von Doenhoff, 1959). Very early tests showed the efficiency of rounded, sharp leading and trailing edges. The demand for more aerodynamic performance wings and the ambiguity of the theories at the time led to tests of numerous wings with improved shapes because of experience. The work of Eiffel and RAF has been recorded as an output of this approach. Driven by First World War, tests were done at Gottingen (Abbott and Von Doenhoff, 1959). These tests contributed significantly to the development of the airfoil design. Most of the proceeding works were derived from the work conducted at Gottingen. Many families were tested in laboratories in different countries, but the work of National Advisory Committee for Aeronautics (NACA) was excellent, including NACA four-, five- and six-digit families. For that, NACA airfoils were always of interest (Abbott and Von Doenhoff, 1959; Riegels, 1961).

Some methods could help suggest a new airfoil, including experimental end numerical ones, by changing the airfoil shape and dimensions such as chord length, upper surface length and curvature and lower surface shape and curvature. However, many airfoil shapes must be investigated for aerodynamic forces (i.e. lift and drag). To tackle this issue, implementing optimization techniques could suggest a desired design. Optimization techniques have been used in numerical airfoil design for a notable time, starting with the initial contributions in the 1970s from researchers such as Hicks and Henne (1978) and Vanderplaats (1979). These advancements were made possible by developing computationally powerful tools that could simulate aerodynamic flows repeatedly. The optimization of numerous parameters affecting the aerodynamic shape was made possible by these computer capabilities, which allowed for iterative performance improvements.

Aerodynamic shape optimization (ASO) has grown significantly over time, incorporating several innovations. Instead of having a single, conclusive solution, an aircraft's design, including its airfoils, is often characterized by an iterative and interrelated process (Berkenstock *et al.*, 2022). Due to the interdependence of various components, a thorough examination of the design space is required, where iterative adjustments and improvements are made. Researchers used different parameterization techniques, such as Bezier curves and B-splines (Fuglsang and Bak, 2004; Rajnarayan *et al.*, 2018; Zhang *et al.*, 2023) and the PARSEC method (Shahrokhi and Jahangirian, 2007). Also, the reviews of Ahamad and Channiwala (2014), Masters *et al.* (2015), Sobieczky (1999) discussed these techniques. To this end, aerodynamicists and designers need to use handy tools to iterate. Berkenstock *et al.* (2022) proposed a convex optimization scheme that used the linear flow theory as a mathematical base for the convex optimization problem, leveraging the super beneficial characteristics of convex optimization. They used polynomial airfoil parameterization (Berkenstock *et al.*, 2022) and cubic splines parameterization (Berkenstock *et al.*, 2023) while still holding the convexity behavior.

Convex optimization techniques have drawn much interest in research, such as control theory (Nonhoff and Müller, 2022; Singh *et al.*, 2017; Zhu *et al.*, 2015) and machine learning (Bubeck, 2015). When functioning within the parameters of convex functions that may be used to describe simplified physics, convex optimization offers the advantage of solving for verified global optima. This characteristic ensures that the solutions found for the given problem are locally and globally optimal. Also, effective convex optimization solvers are widely available (Diamond and Boyd, 2016; Grant and Boyd, 2014). Even on ordinary laptop computers, these solvers displayed exceptional computational efficiency, solving issues involving numerous design parameters under some constraints. However, in specific cases such as aerodynamics, the limitations of the convex constraint and objective functions exclude the complexities modeled by the partial

differential equations that can describe the flow field with more comprehensive and higher fidelity representation.

Computational fluid dynamics (CFD) is essential for optimizing airfoil design because it accurately predicts aerodynamic forces and allows for extensive simulations before wind tunnel testing. CFD, in conjunction with methods such as complex shape parameterization (Deng *et al.*, 2022; He *et al.*, 2019), surrogate models (Li *et al.*, 2019; Siegler *et al.*, 2016) and effective gradient computing (Tyan *et al.*, 2013), has driven significant advancements in ASO. Also, CFD has been used for airfoil analysis in many studies, such as Dumon *et al.* (2019); Gleize *et al.* (2021); and Nived *et al.* (2021).

Based on the open literature and to the best of the authors' knowledge has been, there is no suggested airfoil to replace NACA 64a210 for better aerodynamic performance. Thus, this study aims to propose a new airfoil with better aerodynamic performance than NACA 64a210 for fighters. The study starts with employing the convex optimization approach to obtain an optimal airfoil having a similar cross-sectional area to the famous NACA 64a210 airfoil but with enhancing the thermodynamic forces. The linear theory method is used to model aerodynamic forces. Once the optimal airfoil shape is obtained, a massive verification and investigation are implemented by CFD to analyze the performance of the new airfoil because linear has some limitations. ANSYS Fluent software is used as a CFD tool. The results are compared against the known lift-over-drag data of NACA 64a210 to demonstrate the enhancements provided by the suggested airfoil.

This is quite a fast framework; on a personal computer, it can be run in fractions of a second by using linear flow theory. Our design shows considerable improvements in the airfoil supersonic performance for some flight conditions, which have been validated using CFD. By maintaining the same area and the maximum thickness, we still ensure that the optimized airfoil is manufacturable and can be integrated into current airplanes without sacrificing fuel capacity or structural integrity. This research provides a valuable tool for designing high-speed aircraft that can balance aerodynamic efficiency and real-world engineering requirements with a fast and easy-to-interpret framework that enables multiple trials and troubleshooting.

2. System description and model method

The airfoil general description can be found in Figure 1. The upper surface, also known as the suction surface, is typically related to higher velocity and lower static pressure. On the contrary, the lower surface, also known as the pressure surface, has significantly higher static pressure than the suction surface. The lift force produced by a specific airfoil is influenced by the pressure gradient between these two surfaces. The front point of the airfoil with the greatest curvature (minimum radius) is known as the leading edge. The point of greatest curvature at the back of the airfoil is known as the trailing edge. The line that connects the leading and trailing edges is known as the chord line (Houghton and Carpenter, 2003; Hurt, 1965). The camber and thickness of an airfoil are two crucial factors in describing its shape, as shown in Figure 1.

The models used in this study are the linear theory, optimization and CFD. Everyone is described in the following subsections.

2.1 Airfoil polynomial representation

Because the linear theory and optimization method depend on the geometry of the airfoil as inlet parameters, it is essential to develop a model with tunable parameters for the airfoil shape. Polynomial equations for airfoil parameterization are used in this study. The airfoil is represented by two polynomials that define both the upper and lower surfaces:

$$y_u(x) = \sum_{i=0}^{n} a_i x^i \text{ and } y_l(x) = \sum_{i=0}^{n} b_i x^i \quad (1)$$

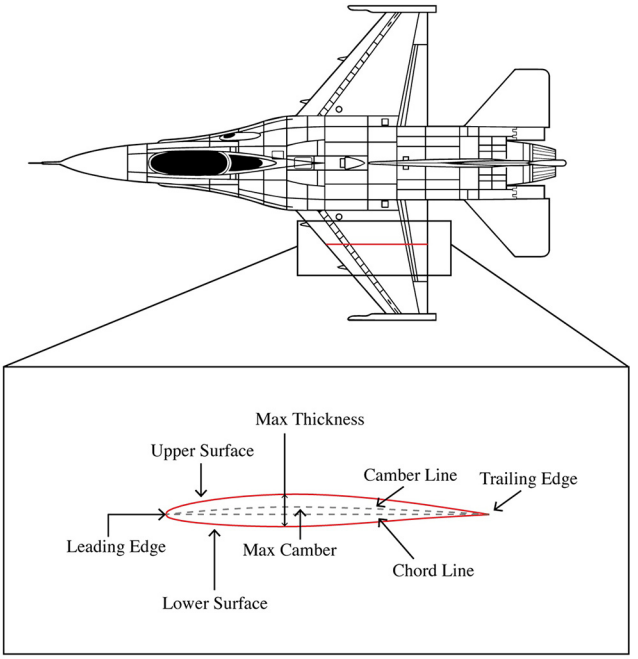

Note: The aircraft blueprint is retrieved from NASA
Source: By authors

Figure 1. Airfoil general description

where a_i and b_i are the upper and lower surfaces' polynomial coefficients. For i = 3, the equations are given by:

$$y_u(x) = a_3x^3 + a_2x^2 + a_1x + a_0 \text{ and } y_l(x) = b_3x^3 + b_2x^2 + b_1x + b_0 \tag{2}$$

To ensure a closed airfoil, the following boundary conditions should be satisfied:

$$y_u(0) = y_l(0) = 0 \text{ and } y_u(c) = y_l(c) = 0 \tag{3}$$

where c is the airfoil chord length and is assumed to have a length of unity. With these boundary conditions satisfied, equation (2) becomes:

$$y_u(x) = -(a_1 + a_2)x^3 + a_2x^2 + a_1x \text{ and } y_l(x) = -(b_1 + b_3)x^3 + b_2x^2 + b_1x \tag{4}$$

So, the problem is characterized by four coefficients (a_1, a_2, b_1 and b_2) $\subset \mathbb{R}^4$. With this infinite space of potential airfoils parameterized using a cubic polynomial to find the combination of design variables that either maximize or minimize certain cost functions as guaranteed by the convex optimization approaches.

The aerodynamic characteristics of airfoils are represented by polynomials under various flow regimes (i.e. subsonic and supersonic). To do so, the principle of thin airfoil theory is used. It is critical to ensure that the airfoil camber and the thickness of the airfoil are relatively smaller than

the chord length. Moreover, the leading-edge radius should be considered small. By complying with these requirements, the thin airfoil theory is applied to examine the properties of airfoils characterized by cubic polynomials in the different subsonic and supersonic flow regimes.

2.1.1 Linear theory and aerodynamic properties for subsonic flows. Thin airfoil theory provides analytical solutions expressed in a simple form for the moment and lift coefficients of an airfoil with a relatively small thickness, operating in a subsonic flow condition with the inviscid, irrotational and incompressible flow. The camber line shape of the airfoil has the sole influence on the sectional moment and coefficients:

$$z(x) = \frac{y_u(x) + y_l(x)}{2} = \frac{-(a_1 + a_2 + b_1 + b_2)x^3 + (a_2 + b_2)x^2 + (a_1 + b_1)x}{2} \tag{5}$$

As stated in Moran (2003), the lift coefficient is $c_l = (\alpha - \alpha_{l0})(2\pi)$ where α_{l0} is the angle of attack corresponding to the zero lift and defined as:

$$\alpha_{l0} = \frac{1}{\pi}\int_0^\pi \frac{dz}{dx}(1 - \cos\theta)d\theta \tag{6}$$

The slope of the camber line can be derived as:

$$\frac{dz}{dx} = \frac{-3(a_1 + a_2 + b_1 + b_2)x^2 + 2(a_2 + b_2) + (a_1 + b_1)}{2}$$

To evaluate the integration in equation (6), we will use the cosine transformation by replacing $x = \frac{1}{2}(1 - \cos\theta)$. So that:

$$\frac{dz}{dx} = (a_1 + a_2 + b_1 + b_2)\left(3\sin^4\frac{\theta}{2} - 1\right) - (a_2 + b_2)\cos\theta$$

Equation (6) becomes:

$$\alpha_{l0} = -\frac{1}{16}(7a_1 + 3a_2 + 7b_1 + 3b_2) \tag{7}$$

So:

$$c_l = 2\pi\left\{\alpha + \frac{1}{16}(7a_1 + 3a_2 + 7b_1 + 3b_2)\right\} \tag{8}$$

For the moment coefficient:

$$c_m = \frac{-1}{2}\int_0^\pi \frac{dz}{dx}(\cos\theta - \cos 2\theta)d\theta \tag{9}$$

Using equation (9):

$$c_m = -\frac{\pi}{64}(15a_1 + 7a_2 + 15b_1 + 7b_2) \tag{10}$$

As discussed in Berkenstock *et al.* (2022), c_l, α_{l0} and c_m all are affine in the subsonic regime, assuming thin airfoil condition. As a result, they are regarded as convex functions of angle of attack (AOA) and the polynomial coefficients a_i and b_i. This convexity property still holds true even when higher-order polynomials are used instead of cubic polynomials. In fact, it is still valid as long as, $y_u(x)$ and $y_l(x)$ are linear in terms of a_i and b_i. Consequently, the functions $(1, x, x^2, x^3)$ can be substituted with any continuous set of functions.

2.1.2 Linear theory and aerodynamic properties for supersonic flows. According to Anderson (1982) and Kuethe and Chow (1997), the lift and drag coefficients can be modeled in closed-form expressions using the linearized flow theory and obeying certain assumptions such as small AOA, thickness, camber and sharp leading edges. These approximations aim to reasonably estimate the aerodynamic characteristics under the given conditions:

$$c_l = \frac{4\alpha}{\sqrt{M^2-1}} \text{and} c_d = \frac{4}{\sqrt{M^2-1}}\left(\alpha^2 + \Lambda_1 + \Lambda_2\right) \tag{11}$$

Here, Λ_1 denotes as a mathematical representation of wave drag coming from the camber line and Λ_2 represents a wave drag created by the airfoil thickness. They both can be modeled as:

$$\Lambda_1 = \int_0^1 \left[\frac{\mathrm{d}}{\mathrm{d}x}\left(\frac{y_u(x)+y_l(x)}{2}\right)\right]^2 \mathrm{d}x$$

$$\Lambda_2 = \int_0^1 \left[\frac{\mathrm{d}}{\mathrm{d}x}\left(\frac{y_u(x)-y_l(x)}{2}\right)\right]^2 \mathrm{d}x$$

Thus, the drag coefficient as a quadratic function in the polynomial coefficient and AOA is expressed as:

$$c_d = \frac{4}{\sqrt{M^2-1}} \begin{bmatrix} \alpha \\ a_1 \\ a_2 \\ b_1 \\ b_2 \end{bmatrix}^{\top} \begin{bmatrix} 1 & 0 & 0 & 0 & 0 \\ 0 & 2/5 & 3/20 & 0 & 0 \\ 0 & 3/20 & 1/15 & 0 & 0 \\ 0 & 0 & 0 & 2/5 & 3/20 \\ 0 & 0 & 0 & 3/20 & 1/15 \end{bmatrix} \begin{bmatrix} \alpha \\ a_1 \\ a_2 \\ b_1 \\ b_2 \end{bmatrix} = \frac{4}{\sqrt{M^2-1}} \boldsymbol{\nu}^{\top} \mathbf{Q} \boldsymbol{\nu} \tag{12}$$

where Q is a positive definite, therefore, c_d is a convex function in v.

Also, the lift-over-drag ratio can be represented as a quadratic over linear function as:

$$\frac{L}{D} = \frac{\alpha}{\boldsymbol{\nu}^{\top} \mathbf{Q} \boldsymbol{\nu}} \tag{13}$$

With the same analysis as above, the lift-over-drag ratio can be convex and representable over the set of $\alpha > 0$.

The linearized flow theory contains several approximations and implicit assumptions, which must be acknowledged. Essential to these assumptions is the principle of an irrotational and inviscid flow that simplifies the mathematical analysis and enables analytical closed-form solutions. In addition, reasonable mathematical simplifications have been deftly adopted to efficiently handle both the completely subsonic and supersonic flow cases. Interested readers may refer to Chapter nine of Anderson (1982).

Those simplifications discussed above, although facilitating a simple framework, need thorough validation to establish their efficacy. Consequently, it is commanding to conduct comprehensive assessments examining the performance of the linear flow theory compared to numerical methods used to solve the complete set of governing equations. Through such investigations, a more comprehensive understanding of the accuracy and limitations of the linear flow theory can be attained.

2.2 Convex optimization

The method of convex optimization is formulated as:

$$\begin{array}{ll} \text{minimize}_x & g_0(x) \\ \text{subject to} & g_i(x) \le 0,\ i = 1,\ \ldots,\ m \end{array} \tag{14}$$

where g_i: $\mathbb{R}^n \to \mathbb{R}$ is a set of convex objectives ($i = 0$) and constraints ($i = 1, 2, \ldots$) functions, and $x \in \mathbb{R}^n$ is a vector of optimization variables. The function is called convex if it obeys the following:

$$g\left(\lambda x + (1-\lambda)y\right) \le \lambda g(x) + (1-\lambda)g(y) \tag{15}$$

Graphically speaking, with $0 \le \lambda \le 1$, the function is convex if it lies below its secant lines. For further discussion regarding convexity, please refer to Boyd and Vandenberghe (2004).

2.3 Optimization constraints

The set of constraints is adopted from Berkenstock *et al.* (2022). The constraints used in this study are minimum area, thickness, internal payload and subsonic lift and moment constraints. The latter two are discussed earlier in the paper and the rest will be discussed in the following subsections.

2.3.1 Minimum area. The airfoil's enclosed area has a substantial impact on its payload capacity. This area is also used to determine, in part, how deep the airfoil section is structural. The enclosed area is calculated mathematically by integrating the difference between the lower and upper surfaces over the whole airfoil span. The integral has the form of:

$$A = \int_0^1 \left(y_u(x) - y_l(x)\right)\mathrm{d}x = \frac{1}{12}(3a_1 + a_2 - 3b_1 - b_2) \ge A_{min} \tag{16}$$

This leads to an affine constraint.

2.3.2 Thickness. It is often of interest to have a certain airfoil thickness. This can be either specified through the entire chord or on a specific segment $x \in [x_1,\ x_2]$. The corresponding constraint function is:

$$u(x) = -(a_1 + a_2 - b_1 - b_2)x^3 + (a_2 - b_2)x^2 + (a_1 - b_1)x \tag{17}$$

2.3.3 Internal payload. A circular payload constraint can be added to guarantee a place in any location. For instance, by adding the following sampled constraints, it is possible to include a circle with radius r and center $[x_c, y_c]$. These restrictions apply to the airfoil's upper and lower surfaces:

$$u(\theta) = \begin{cases} -(a_1 + a_2)K^3 + a_2K^2 + a_1K - y_c - r\sin\theta) \ge 0\ \forall\theta\in[0,\ \pi] \\ -(b_1 + b_2)K^3 + b_2K^2 + b_1K - y_c - r\sin\theta) \le 0\ \forall\theta\in[\pi,\ 2\pi] \end{cases} \tag{18}$$

where, $K = (x_c + r\cos\theta)$.

2.4 Optimization algorithm verification

The algorithm is originally presented in Berkenstock *et al.* (2022), which is also used to verify the algorithm implementation in this paper. Exact results are obtained compared to results of the same reference, as shown in Table 1.

As shown in Table 1, there is an excellent agreement between our results and the results obtained by the authors of Ref. Berkenstock *et al.* (2022).

Table 1. Verification of the algorithm's findings of the present study and those of Berkenstock *et al.* (2022)

Case	Literature (Berkenstock *et al.*, 2022)	Present study
Minimum drag supersonic airfoil	$\alpha = 0°$ $a_1 = 0.2250$ $a_2 = -0.2250$ $b_1 = -0.2250$ $b_2 = 0.2250$	$\alpha = 0°$ $a_1 = 0.2250$ $a_2 = -0.2250$ $b_1 = -0.2250$ $b_2 = 0.2250$
Maximum lift-to-drag ratio supersonic airfoil with internal payload	$a = 11.17°$ $a_1 = 0.5240$ $a_2 = 1.010$ $b_1 = -0.5240$ $b_2 = -1.010$	$a = 11.3045°$ $a_1 = 0.5239$ $a_2 = 1.0086$ $b_1 = -0.5239$ $b_2 = -1.0086$
Maximum lift-to-drag ratio supersonic airfoil with subsonic lift and moment constraints	$\alpha = 18.3300°$ $a_1 = 0.4500$ $a_2 = -0.6300$ $b_1 = -0.6000$ $b_2 = 1.3900$	$\alpha = 18.3690°$ $a_1 = 0.4513$ $a_2 = -0.6319$ $b_1 = -0.5976$ $b_2 = 1.3857$

Source: Table by authors

2.5 Application to NACA 64a210 optimization

The airfoil, NACA 64a210, is aimed to be modified for better aerodynamic performance. NACA 64a210 belongs to the NACA 6 series, and the new optimized airfoil could be named modified NACA 64a210. Using the abovementioned convex constraints, the lift-over-drag ratio is the prime objective target for the specified airfoil, and this quantity should be maximized. So, for the optimization problem, we will minimize the reciprocal of the quantity in equation (13). The airfoil coordinates are retrieved from Loftin (1946). The problem is formulated as:

$$
\begin{aligned}
&\underset{[v, x_c, y_c]}{\text{minimize}} && \frac{\boldsymbol{v}^{\top}\boldsymbol{Q}\boldsymbol{v}}{\alpha} \\
&\text{subjectto} && \min_{x\in[0,1]} \left(-(a_1 + a_2 - b_1 - b_2)x^3 + (a_2 - b_2)x^2 + (a_1 - b_1)x \right) \geq 0 \\
& && \max_{x\in[0,1]} \left(-(a_1 + a_2 - b_1 - b_2)x^3 + (a_2 - b_2)x^2 + (a_1 - b_1)x \right) \leq \zeta_{max} \\
& && \min_{\theta\in[0,\pi]} \left(-(a_1 + a_2)(K)^3 + a_2(K)^2 + a_1(K) - y_c - r\sin\theta \right) \geq 0 \\
& && \max_{\theta\in[\pi,2\pi]} \left(-(b_1 + b_2)(K)^3 + b_2(K)^2 + b_1(K) - y_c - r\sin\theta \right) \leq 0 \\
& && \frac{1}{12}(3a_1 + a_2 - 3b_1 - b_2) \geq A_{min} \\
& && 2\pi\left(\alpha + \frac{1}{16}(7a_1 + 3a_2 + 7b_1 + 3b_2)\right) \geq c_{l_{min}} \\
& && -\frac{\pi}{64}(15a_1 + 7a_2 + 15b_1 + 7b_2) \leq c_{m_{max}} \\
& && \alpha \geq 0.
\end{aligned}
$$

The NACA 64a210 airfoil's area is calculated using numerical integration of the coordinates and is fixed for the optimal one. The coordinates are normalized per chord. Consequently, the

Table 2. Design parameters for optimization based on the area of NACA 64a210

Parameter	Value
Mach	2
Maximum thickness – ζ_{max}	0.1
Payload radius – r	0.04
Payload x location per chord – x_c	0.25
Payload y location per chord – y_c	0
Minimum area – A_{min}	0.0661
Subsonic minimum lift coefficient – $c_{l_{min}}$	1.5
Subsonic maximum moment coefficient – $c_{m_{max}}$	−0.15

Note: All values are normalized such that subsonic lift and moment coefficients are linearized; the rest of the parameters are normalized per chord
Source: Table by authors

rest of the design parameters will be normalized. Table 2. Summarizes the design parameters of the optimization problem. Then, the new airfoil will be tested using CFD tools. The overall process schematic can be shown in Figure 2.

The convex optimization tool known as CVX, developed by Grant and Boyd (2014) package, is a language model that deals with convex optimization. It transforms the problem to the standard form, uses an external solver like SDPT3 (Tutuncu *et al.*, 2003) or SeDuMi (Sturm, 1999) and postprocess the results by overwriting the optimization variable to its optimal numeric

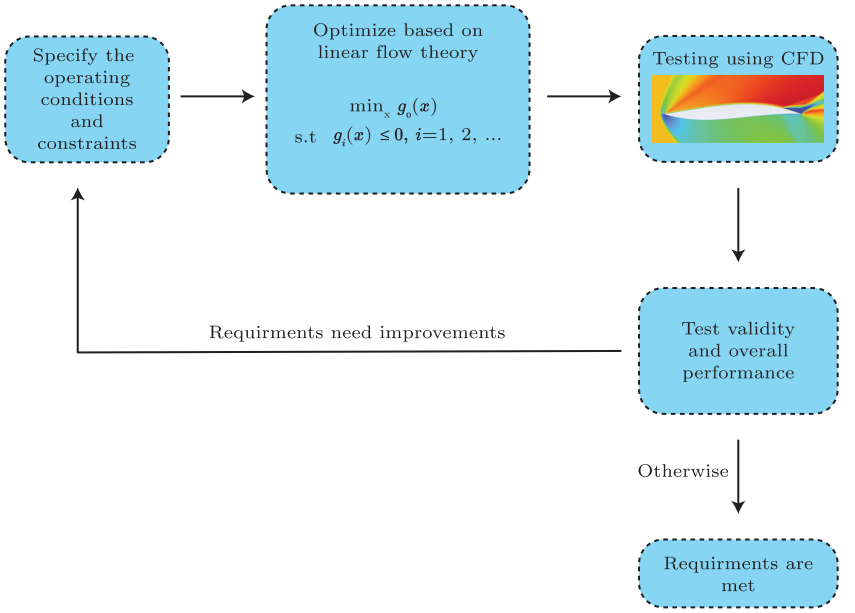

Source: By authors

Figure 2. Overall optimization and CFD testing process schematic

value. Then, the problems' optimal value is assigned to the variable *cvx_optval*. If the problem had been infeasible, a variable called *cvx_status* would have been assigned as *infeasible*, and the optimization variable would have been assigned as NaN. Further details can be found in the tutorial presentation (Boyd and Parrilo, 2009). The package is coupled with MATLAB software to obtain the optimization solution.

3. Computational fluid dynamics model

To verify the accurate performance of the optimal airfoil, the CFD analysis is carried out because the linearized flow method is restricted by many constraints and cannot show the actual performance under different situations. The CFD model is governed by the principles of mass, momentum and energy conservation in addition to the turbulent flow model. The flow is assumed to be steady-state and compressible.

The conservation laws of mass, momentum and energy form the foundational rules of fluid dynamics. The law of mass conservation expressed in the continuity equation shows that the mass inflow and outflow should be balanced in a fluid system, thereby making total mass remain constant. As per Newton's second law of motion, conservation of momentum is that the rate of change of momentum of a body or object is equal to the applied force. Energy conservation conditions demand that the net rate of energy in the system be equal to rates of heat transfer and work done to enable its embodiment of the various contributions in the dynamics of flow. We make use of these basic principles to serve as the basis for the numerical simulation.

For the case of this study, the turbulence model $k - \omega$ shear stress transport (SST) and the Spalart–Allmaras (SA) were tested. $k - \omega$ SST was initially proposed by Menter in 1992 (Menter, 1992). The fundamental idea behind the $k - \omega$ model is to preserve the precise and reliable formulation of the $k - \omega$ model in near wall boundary while using the freestream independence of the $k - \epsilon$ model in the boundary-layer's outer region. The $k - \epsilon$ model is converted into a $k - \omega$ formulation to accomplish this. The additional cross-diffusion element that appears in the $\omega -$ equation and the different modeling constants distinguish this formulation from the original $k - \omega$ model. This model is a two-equation model, the same as the models it is adapted from; the equation can be found in the original source (Menter, 1992). The one-equation SA turbulence model focuses on aerodynamic applications. The SA model provides satisfactory results for various engineering applications, especially for those involving aerodynamics (Wilcox, 2006).

3.1 Model validation

To validate the model used in this study, experimental data from Riegels (1961) for the NACA 0015 airfoil was used at free stream $M = 0.702$ (with sonic flow over the wing) and AOA = −4°. In particular, the present results are compared to experimental data in terms of the pressure coefficient values, as shown in Figure 3. There is an excellent agreement between the experimental and numerical results for both turbulence models. Thus, they can be used for the present study.

The $k - \omega$ SST Model will be used for the rest of the study. The flow behavior of the transonic regime is far more complicated than that of the supersonic regime. Therefore, using the $k - \omega$ SST model for supersonic flow will be sufficient for the purpose of the study. To the best of our search, we cannot find experimental data for the NACA64a210 airfoil. So, we validated the CFD model using the available experimental data.

3.2 Performance indices

As we focus on the lift-over-drag ratio, we will consider the lift-over-drag ratio as a performance index. The performance of the original and new airfoils will be evaluated and

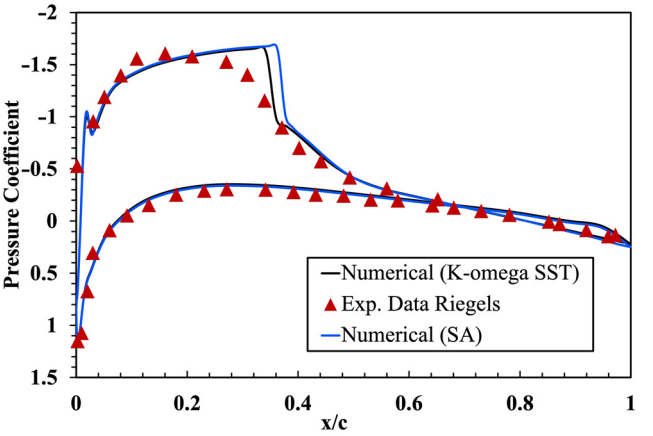

Source: By authors

Figure 3. Pressure coefficient validation against experimental results obtained at AOA = –4° and free stream $M = 0.702$ from (Riegels, 1961)

compared using the proposed metric. By scrutinizing this ratio under various conditions, we can have insights into the efficacy of the optimization.

3.3 Boundary operating conditions

The standard pressure far-field boundary condition is used. The airfoils are investigated using different Mach number values (1.5, 2 and 2.5), and for each case, the values of the AOA are scanned from [0°, 20°]. Moreover, the optimized airfoil is assessed under different scenarios compared to the original NACA 64a210 airfoil.

3.4 Mesh independence

Under typical pressure far-field boundary circumstances, the two-dimensional conventional C-shaped domain was discretized into a mesh, and grid independence was examined for the newly designed airfoil (Figure 4).

The inlet Mach number was set to 2, the inlet temperature was 300 K and the far pressure was at 101.3 kPa. The lift and drag coefficients were calculated for four meshes with varied element counts (111,900, 260,200, 302,940 and 314,600) to determine how sensitive the results were to mesh density. Table 3 gives an overview of these various mesh study scenarios.

Figure 5 shows a graphical representation of each scenario's lift and drag coefficients. The changes in the values of lift and drag coefficients between various scenarios are found to be within an acceptable range of error after looking at the data presented in Table 3 and the associated Figure 5. In consideration of computational time, we utilized mesh case number 2 (with 260200 elements) for the remaining simulation scenarios.

4. Results and discussion

4.1 Optimal airfoil from linear flow theory

The parameters presented in Section 2.5 result in the optimized parameters such as:

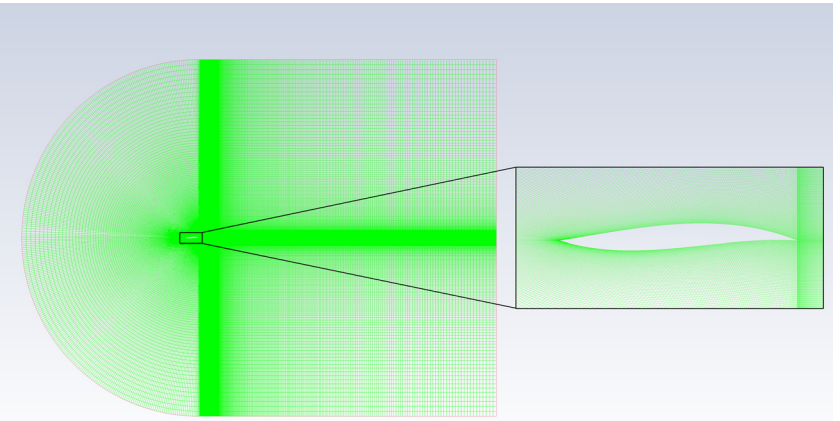

Source: By authors

Figure 4. The mesh shape and sizing for the optimized airfoil

Table 3. Mesh independence study with a different number of elements with fixed AOA = 0^{o} and Mach number = 2

Case no.	No. of elements	Lift coefficient	Drag coefficient
1	111,900	−0.0213	0.0475
2	260,200	−0.0208	0.0477
3	302,940	−0.0207	0.0477
4	314,600	−0.0207	0.0477

Source: Table by authors

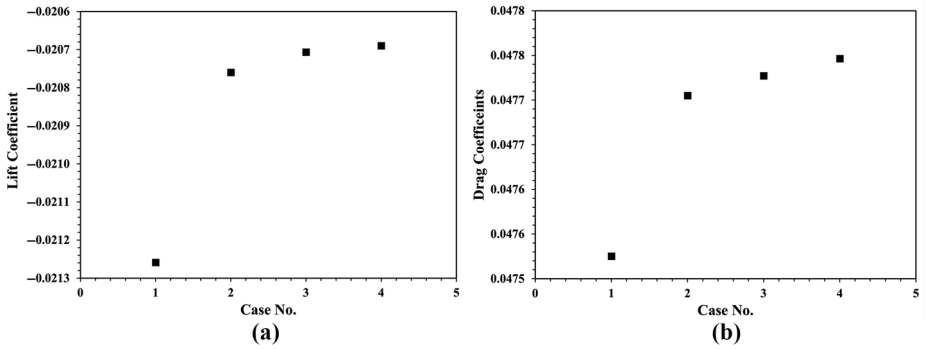

Source: By authors

Figure 5. (a) Lift and (b) drag coefficients for each meshing case

$$\nu = \begin{bmatrix} \alpha \\ a_1 \\ a_2 \\ b_1 \\ b_2 \end{bmatrix} = \begin{bmatrix} 0.1639 \\ 0.1562 \\ 0.0821 \\ -0.3058 \\ 0.6749 \end{bmatrix}$$

We used the SDPT3 solver from the CVX library; the convergence curves of primal and dual infeasibilities, as well as the duality gap, are presented in Figure 6. If the max(relative gap, infeasibilities) $< \epsilon$ where ϵ is a very small number, a stopping criterion is met indicating the convergence of the algorithm.

The algorithm runs for 24 iterations to reach the termination criterion with an overall central processing unit (CPU) time of 0.25 s on an M2 MacBook Air with an average of 0.01 s per iteration, highlighting the algorithm's speed efficacy on a personal computing unit. The results mean that the airfoil will operate optimally at $\alpha = 0.1639°$ and rad = 9.3908° with the lift-over-drag ratio of 3.5039, which will be validated using CFD in the upcoming subsection. Also, the optimized airfoil can be found in Figure 7.

Despite upholding the same area and maximum thickness as the NACA 64a210 airfoil, the new airfoil assures a better performance than the NACA 64a210 airfoil. Moreover, the lift-over-drag ratio reliably outweighs that of the NACA 64a210 airfoil under the same operating conditions.

4.2 Numerical results

The contour plots of the velocity, temperature and pressure of the new airfoil are depicted in Figures 8 and 9 at operating Mach = 1.5 and 2.0, respectively. In Figures 8 and 9, the velocity values are higher above the airfoil for AOA = 9° due to more sucking and more pressure generated at the lower surface, which faces the flow directly. It is worth noting that AOA is changed by the flow direction in the CFD simulation; thus, the airfoil's shape is kept horizontal in the figures. In the first case (AOA = 0°) Figures 8(a), (c) and (d) and 9(a), (c) and (d), the oblique shockwaves appear over upper and lower surfaces starting from the

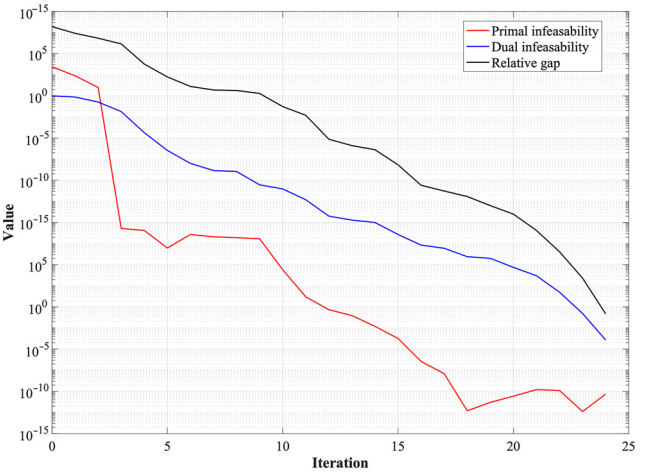

Source: By authors

Figure 6. The convergence curves of the primal and dual infeasibility and the relative gap

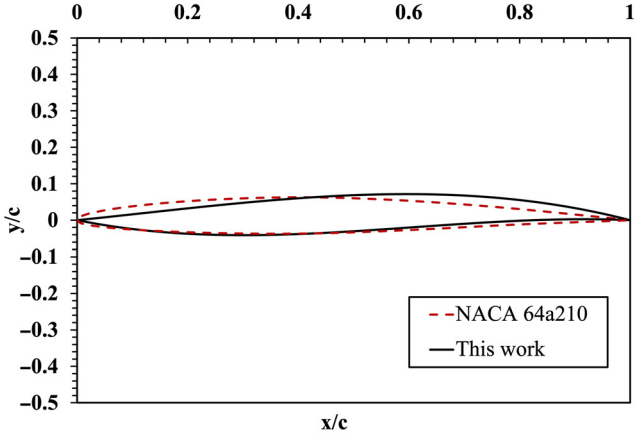

Source: By authors

Figure 7. The optimized airfoil geometry using the design parameters in Table 1

leading edge, while an expansion shockwave appears with the airfoil curvature on the upper surface closer to the tailing edge, which helps increase the velocity and generates some lift. Also, one can see that as the free stream Mach number increases, the oblique shock wave angle gets smaller. For example, we consider Figures 8(a) and 9(a), at the leading edge, the deflection angle is held fixed as they both experience the same AOA; however, the Mach number changes from 1.5 in Figure 8(a) to 2 in Figure 9(a). Thus, this corresponds to a less oblique shock wave angle – see Anderson (1982).

In contrast, the case of AOA = 9° has an oblique shock wave under the lower surface and an expansion wave over the upper surface, which is expected to generate more lift but also more drag, as shown in Figure 10(a) and (b). Due to the occurrence of the oblique shockwave, Figures 8(c) and (d), and 9(c) and 9(d) show that the pressure is high around the airfoil closer to the leading edge for AOA = 0° and under the lower surface of the case of AOA = 9°. However, the pressure is very low over the upper surface of the case of AOA = 9° due to the expansion waves, which helps to produce more lift. Any AOA > 0o is expected to have a similar distribution of oblique and expansion waves over the airfoil to those of AOA = 9° with lower values and lower shock angles. Also, Figure 8(d) and 8(e), and Figure 9(d) and 9(e), show that the temperature values are high for low-velocity values in the case of expansion waves under the lower surface when the angle of attack > 0°. The maximum temperature is generated at the leading edge due to stagnation. Also, temperature rises at the tailing edge due to generating a new oblique shockwave, which could reduce the lift profile in this region.

A more in-depth look at the behavioral analysis of the flow around the airfoil, we have noticed a small, localized region of flow separation at the trailing edge starts to appear when the optimized airfoil operates at Mach number of 1.5, which aligns with what we have expected given the increased AOA. In Figure 10(a), we have observed a slight pressure increase on the upper surface, which can be justified by the circulation flow at this location, as depicted in Figure 10(b). Furthermore, as seen in Figure 8(d), we can say that the flow at this region experiences an early oblique shock wave as a natural adjustment to equate the upper surface pressure with the lower surface one, as indicated by the clearly observable slip-line. Conversely, the behavior changes with $M = 2$, as depicted in Figure 9(d); we also expect

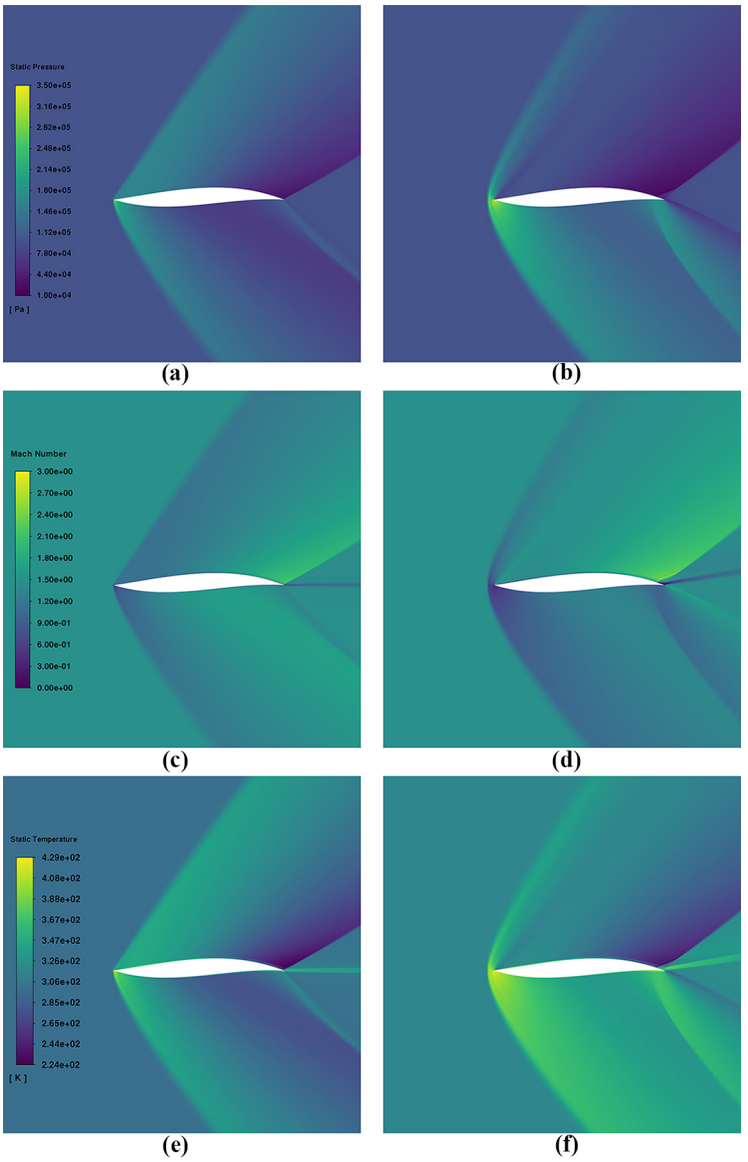

Notes: (a); (b) represent the contours of pressure at AOA = 0° and 9°, respectively; (c); (d) illustrate the contours of the Mach number at AOA = 0° and 9°, respectively; and finally; (e); (f) illustrate the contours of the temperature at AOA = 0° and 9°, respectively
Source: By authors

Figure 8. Different contour plots showcasing the optimized airfoil at M = 1.5

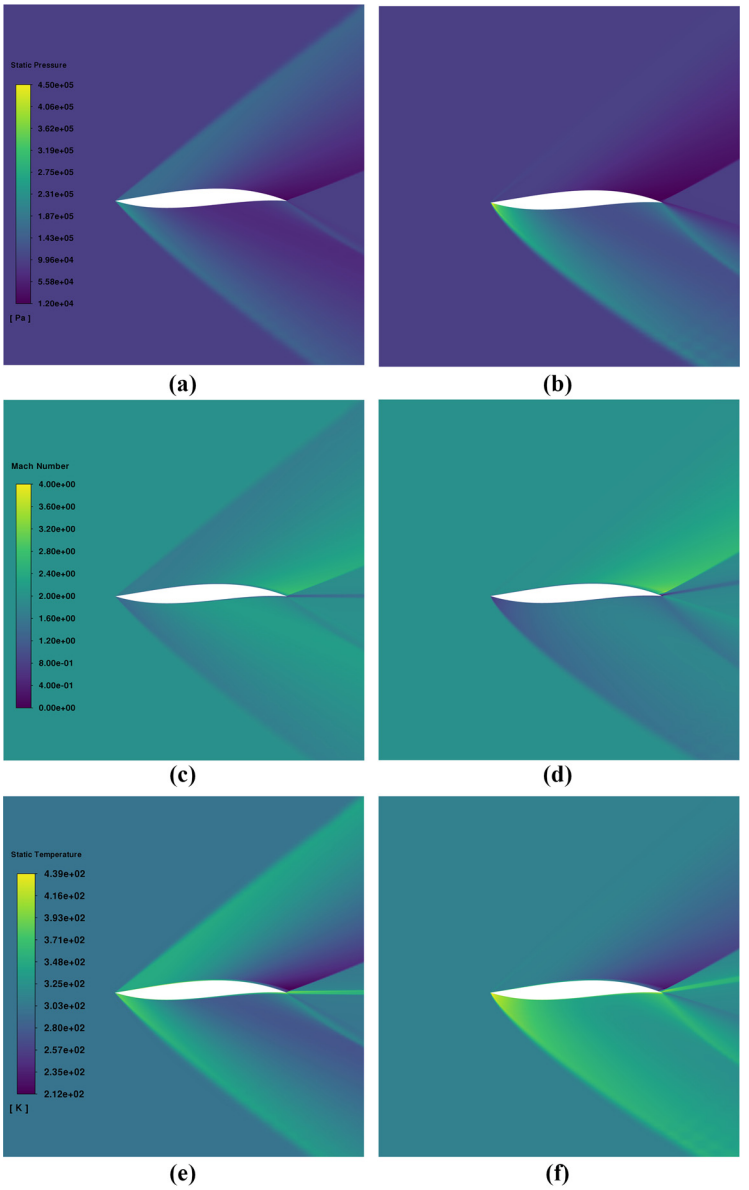

Notes: (a); (b) represent the contours of pressure at AOA = 0° and 9°, respectively; (c); (d) illustrate the contours of the Mach number at AOA = 0° and 9°, respectively; and finally; (e); (f) illustrate the contours of the temperature at AOA = 0° and 9°, respectively
Source: By authors

Figure 9. Different contour plots showcasing the optimized airfoil at $M = 2.0$

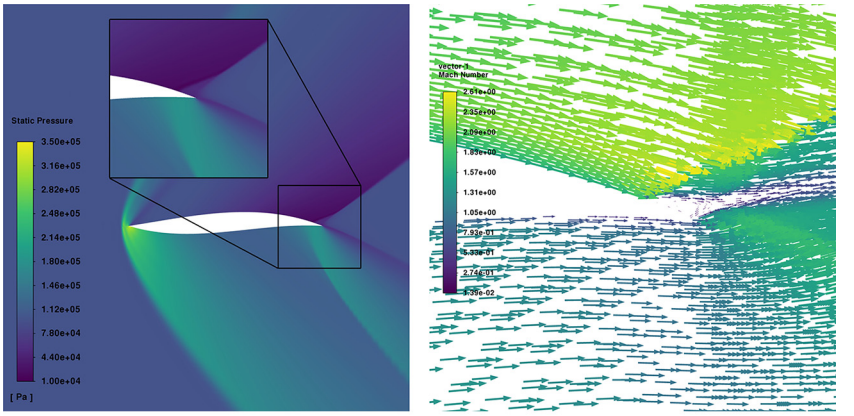

(a) **(b)**

Source: By authors

Figure 10. (a) Represents the pressure contours of the optimized airfoil with operating Mach = 1.5 and at AOA = 9°. (b) Represents the flow behavior at the trailing edge with the same operating conditions

the same behavior with higher Mach numbers. As the Mach number increases, the shock wave lags until it occurs at the leading edge. The airfoil response to the change in AOA in terms of flow separation is good, as the separation occurs near the trailing edge. This indicates a not-so-effective rise in the pressure on the upper surface, which does not affect the lift and the drag that much when operating at high Mach numbers.

Compared to Figure 10(a), (d) and (e), Figure 11 shows a notable difference in that the NACA 64a210 airfoil experienced a detached shock wave even from AOA = 0°, unlike the case of this work's airfoil. This can be justified due to NACA's blunt leading edge. For AOA = 0° with M = 1.5, the lift-over drag ratio experienced a significant percentage increase, as shown in Figure 13, due to the difference in the kind of shock wave experienced by the two airfoils, attached obliquely for our work and detached shock for NACA's work. One edge for the new airfoil is that it has the same area and, in turn, the same weight as the NACA 64a210, with noticeable improvement in the aerodynamic performance indicative of its suitability for supersonic flights.

Figure 12 shows the details of the essential forces to evaluate the present airfoil against NACA 64a210 airfoil under different conditions. The comparative study of the new airfoil and the NACA 64a210 airfoil shows that the optimized airfoil reveals a notable decrease in drag coefficient throughout the entire space of tested Mach numbers in the supersonic regime and angles of attacks. Also, the lift coefficient exhibits some enhancement. One can see that the smooth and thin shape of the leading edge of the new airfoil compared to the old one in Figure 7 may have an impact on drag reduction, as depicted in Figure 12(c). In turn, the lift-over-drag ratio experiences a considerable increase when compared to the NACA 64a210 airfoil. It is worth noting that the linear flow theory prediction of the optimal lift-over-drag ratio was equal to 3.5039 at an angle of attack of 9.3908° matching what has been found from the comprehensive CFD study [see Figure 12(c)], and this optimal value of the lift-over-drag is independent of the operating Mach number in the supersonic flow regime as also predicted by equation (13). This is as well verified by the CFD study as shown in Figure 13 for different M values, demonstrating the linear flow theory robustness to predict the aerodynamic performance at the optimal AOA.

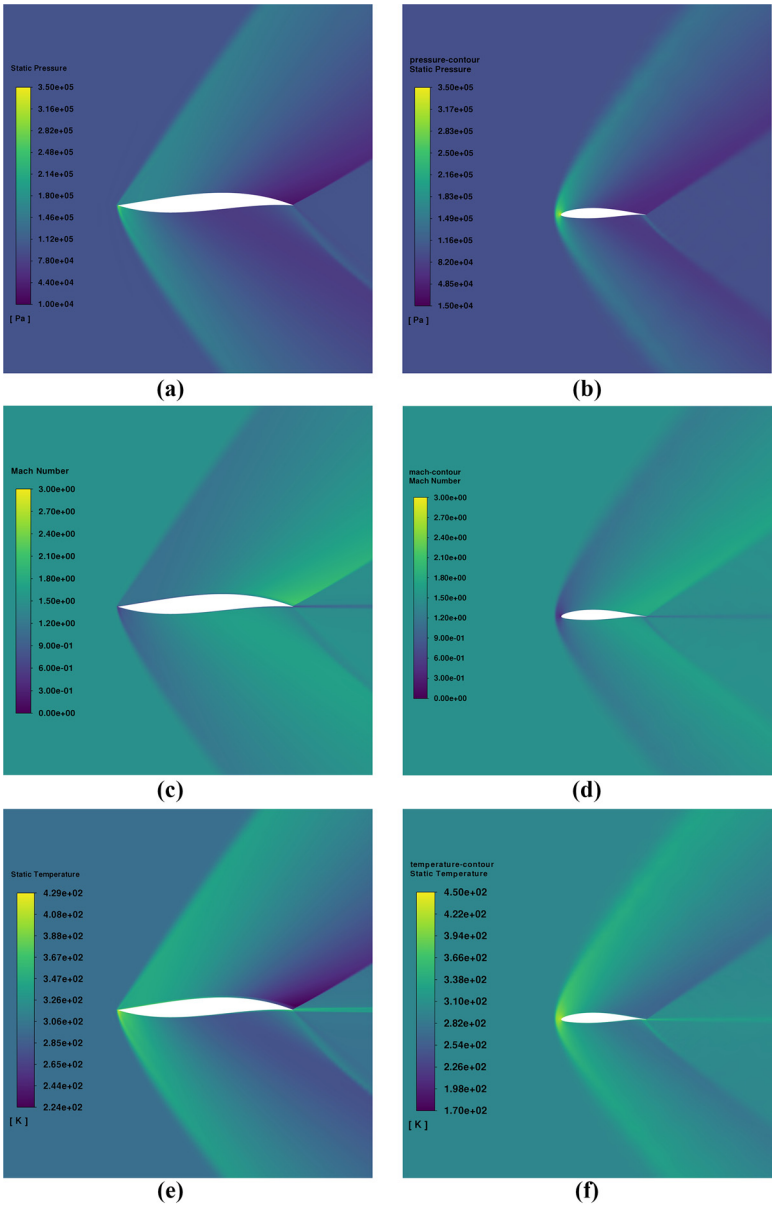

Notes: (a); (b) show the pressure contours; (c); (d) show the Mach number contours; (e); (f) show the temperature contours. All of them captured at M = 1.5 and AOA = 0°
Source: By authors

Figure 11. The contour plots for NACA 64a210 airfoil juxtaposed against the contours of the optimized airfoil

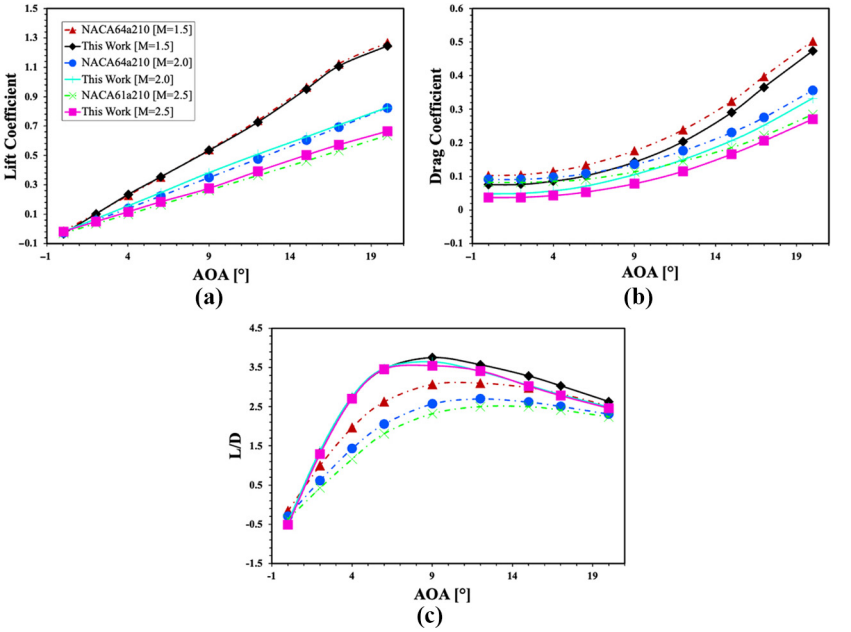

Note: The comparison highlights the difference between drag and lift coefficients for both airfoils with different AOAs at Mach numbers of 1.5, 2, and 2.5. Also, a comparison between the lift-over-drag ratios is shown
Source: By authors

Figure 12. Comparison between the original NACA 64a210 airfoil and the resulting airfoil of this study

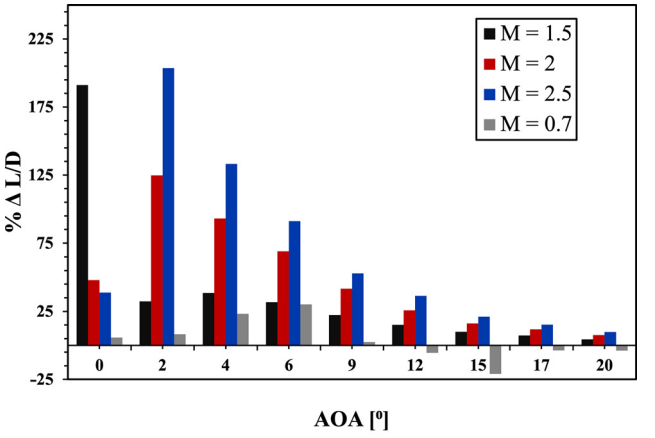

Source: By authors

Figure 13. The percentage increase of the optimized airfoil shape as compared to the original NACA 64a210 airfoil at different AOAs and Mach numbers

The present airfoil substantially enhances the lift-over-drag ratio, mainly by reducing the drag and, to some extent, enhancing the lift due to changes in the geometry and thinning of the leading edge. Moreover, Figure 13 evaluates the percentage increase in the lift-over-drag for the supersonic flow regime (the regime of interest) and a studied case of the subsonic regime of the present airfoil against the NACA 64a210 airfoil. It should be noted that as the angle of attack rises, the increment in the lift-to-drag ratio becomes less noticeable; the incremental gains in lift start to fall behind the high rise in drag value. However, through the entire supersonic domain of the investigated operating conditions, a significant percentage increase in the lift-over-drag ratio is experienced for the new airfoil compared to the NACA's airfoil. For example, the comparison between the two airfoils across the tested supersonic range of Mach numbers resulted in lift-over-drag ratio enhancements between 4.4% - 191.1% at M = 1.5, 7.1% - 124.8% at M = 2 and 9.8% - 203.5% at M = 2.5 depending on the angle of attack. Thus, the improvement in the lift-over-drag ratio is of great significance as it directly impacts energy consumption. Although our method was used initially for the supersonic regime up to this point (future constraints, in a sense that will be discussed in the sequel, shall be developed to have good subsonic behavior throughout the entire regime), we have tested our method on a subsonic case, at which many fighters may cruise with M = 0.7. In addition to Figure 13, we present further results for the subsonic case in Table 4. Across the entire range of operating AOAs in the subsonic case, the NACA 64a210 consistently demonstrated higher lift coefficients than our design.

Conversely, from 0 to 20 degrees AOA, except for the case of 15 degrees, our design exhibited lower drag coefficients compared to the NACA's. This reduction in drag resulted in an

Table 4. A comparison between the present work's airfoil and NACA 64a210 in subsonic case with $M = 0.7$

AOA	Airfoils	Cl	% Δ Cl	Cd	% Δ Cd	L/D	%Δ L/D
0	Ours	0.3750	↓11.0219	*0.0111*	↑15.8738	*33.8402*	↑5.7673
	NACA's	*0.4215*		0.0132		31.9949	
2	Ours	0.5730	↓19.9473	*0.0176*	↑26.0020	*32.5635*	↑8.1822
	NACA's	*0.7158*		0.0238		30.1006	
4	Ours	0.7327	↓20.0205	*0.0299*	↑35.1185	*24.5069*	↑23.2701
	NACA's	*0.9161*		0.0461		19.8806	
6	Ours	0.8224	↓5.4306	*0.0514*	↑27.2910	*15.9991*	↑30.0657
	NACA's	0.8696		0.0707		12.3008	
9	Ours	0.8358	↓2.7456	*0.1131*	↑5.0340	*7.3886*	↑2.4097
	NACA's	0.8594		0.1191		7.2148	
12	Ours	0.7691	↓10.8833	*0.1741*	↑5.6730	*4.4163*	↓5.5237
	NACA's	0.8630		0.1846		*4.6745*	
15	Ours	0.7901	↓12.5591	0.2605	↓10.7152	3.0326	↓21.0218
	NACA's	*0.9036*		*0.2353*		*3.8397*	
17	Ours	0.8349	↓13.6162	0.2760	↑10.3544	3.0251	↓3.6385
	NACA's	*0.9665*		0.3079		*3.1393*	
20	Ours	0.8681	↓13.9281	*0.3372*	↑10.5586	2.5747	↓3.7673
	NACA's	*1.0085*		0.3770		*2.6755*	

Notes: The table compares lift and drag coefficients and the left-over-drag ratio. Every *bolded* entry is for advantage. The symbol below indicates a decline in our design performance, and the symbol up indicates vice versa

Source: Table by authors

overall increase in the lift-to-drag ratio for our design in most cases. Beyond 12 degrees AOA, while our design still improved the drag coefficient in many cases, the lift coefficient became the dominant factor. In total, our design is still near-by the lift-to-drag ratio as compared to the NACA airfoil, although it is not in the optimal design regime. The decline in lift-to-drag performance for our design at higher AOAs can be attributed to increased flow separation and turbulence. We also note that up to AOA = 12 degrees, our design still operates better than NACA's one in the studied subsonic case, indicative of its good performance.

In Figure 8(b), (d) and (f), we have observed a detached shock wave at high AOAs with M = 1.5. This phenomenon can be attributed to the effect of the AOA on the deflection angle. As the deflection angle increases, it may change the morphology of the shock from being attached to the body into a fully detached shock wave (Anderson, 1982). Figure 13 highlights a notable effect seen at Mach 1.5. In contrast to higher AOAs, the percentage increase in the lift-to-drag ratio shows an unusual significance at AOA = 0° because of the detached shock.

5. Concluding remarks

This paper investigates enhanced fighter airfoil performance by suggesting a new airfoil. A convex optimization method to optimize a fighter airfoil is implemented, and the results are verified and additionally explored by a CFD study using ANSYS Fluent. Although the optimization problem is formulated by using the mathematical framework derived from the linear flow theory, which inherently includes numerous assumptions, a good agreement is found between the linear flow theory and the CFD solution for the optimal results of linear flow theory. That means that despite the inherent assumptions of the linear flow theory, the method can be used confidently as a design method and can facilitate the initial optimization steps to find a global optimal airfoil based on the agreement with the full-fidelity CFD analysis. The typical (NACA 64a210) and optimized airfoils are investigated over the range of the specified Mach numbers and at different AOAs. Under all investigated supersonic Mach numbers and angles of attack, the optimized airfoil outperforms the NACA 64a210 airfoil in terms of the lift-over-drag ratio. For example, compared to the NACA 64a210 airfoil, the present airfoil shows the lift-over-drag ratio increases by 4.4%–191.1% at M = 1.5, 7.1%–124.8% at M = 2 and 9.8%–203.5% at M = 2.5, depending on the angle of attack. On a practical note, the sharp leading and trailing-edged airfoil introduced by our study is well suited for supersonic cruise performance because it has a larger lift-to-drag ratio than the rounded leading edge and sharp trailing edge airfoils. However, we expect the low-speed performance will be affected by the sharp leading edge. Future research will focus on introducing a convex rounded leading edge constraint to consider both supersonic and low-speed performance.

References

Abbott, I. and Von Doenhoff, A. (1959), *Theory of Wing Sections: Including a Summary of Airfoil Data*, Dover Publications, available at: https://store.doverpublications.com/products/9780486605869?srsltid=AfmBOooYaxN_Qq3PVlECdoPDpXwnSpv2AkYwaAwcpBvNCxDJ5KNd4Ckz

Abdulrahman, G.A.Q., Qasem, N.A.A., Imteyaz, B., Abdallah, A.M. and Habib, M.A. (2023), "A review of aircraft subsonic and supersonic combustors", *Aerospace Science and Technology*, Vol. 132, p. 108067, doi: 10.1016/j.ast.2022.108067.

Ahamad, J. and Channiwala, S. (2014), "Airfoil parameterization techniques: a review", *American Journal of Mechanical Engineering*, Vol. 2 No. 4, pp. 99-102, doi: 10.12691/ajme-2-4-1.

Anderson, J.D. (1982), *Modern Compressible Flow, with Historical Perspective*, McGraw-Hill, available at: www.mheducation.com/highered/product/modern-compressible-flow-historical-perspective-anderson/M9781260471441.html#authorbios

Berkenstock, D., Alonso, J.J. and Lessard, L. (2022), "A convex optimization approach to thin airfoil design", AIAA AVIATION 2022 Forum, presented at the AIAA AVIATION 2022 Forum, American Institute of Aeronautics and Astronautics, *Chicago, IL and Virtual*, doi: 10.2514/6.2022-3356.

Berkenstock, D., Alonso, J.J. and Lessard, L. (2023), "A convex optimization approach to thin airfoil design using cubic splines", AIAA SCITECH 2023 Forum, presented at the AIAA SCITECH 2023 Forum, American Institute of Aeronautics and Astronautics, *National Harbor, MD and Online*, doi: 10.2514/6.2023-0651.

Boyd, S. and Vandenberghe, L. (2004), *Convex Optimization*, Cambridge University Press, Cambridge.

Boyd, S. and Parrilo, P. (2009), "Disciplined convex programming and CVX".

Bubeck, S. (2015), "Convex optimization: algorithms and complexity", arXiv, 16 November.

Deng, F., Xue, C. and Qin, N. (2022), "Parameterizing airfoil shape using aerodynamic performance parameters", *AIAA Journal*, Vol. 60 No. 7, pp. 4399-4412, doi: 10.2514/1.J061464.

Diamond, S. and Boyd, S. (2016), "CVXPY: a python-embedded modeling language for convex optimization", *Journal of Machine Learning Research*, Vol. 17, pp. 1-5.

Dumon, J., Bury, Y., Gourdain, N. and Michel, L. (2019), "Numerical and experimental investigations of buffet on a diamond airfoil designed for space launcher applications", *International Journal of Numerical Methods for Heat and Fluid Flow*, Vol. 30 No. 9, pp. 4203-4218, doi: 10.1108/HFF-07-2018-0353.

Fuglsang, P. and Bak, C. (2004), "Development of the Risø wind turbine airfoils", *Wind Energy*, Vol. 7 No. 2, pp. 145-162, doi: 10.1002/we.117.

Gleize, V., Costes, M. and Mary, I. (2021), "Numerical simulation of NACA4412 airfoil in pre-stall conditions", *International Journal of Numerical Methods for Heat and Fluid Flow*, Vol. 32 No. 4, pp. 1375-1397, doi: 10.1108/HFF-07-2021-0514.

Grant, M. and Boyd, S. (2014), "CVX: Matlab software for disciplined convex programming, version 2.1", available at: http://cvxr.com/cvx

He, X., Li, J., Mader, C.A., Yildirim, A. and Martins, J.R.R.A. (2019), "Robust aerodynamic shape optimization—from a circle to an airfoil", *Aerospace Science and Technology*, Vol. 87, pp. 48-61, doi: 10.1016/j.ast.2019.01.051.

Hicks, R.M. and Henne, P.A. (1978), "Wing design by numerical optimization", *Journal of Aircraft*, Vol. 15 No. 7, pp. 407-412, doi: 10.2514/3.58379.

Houghton, E.L. and Carpenter, P.W. (2003), *Aerodynamics for Engineering Students*, Elsevier, available at: https://shop.elsevier.com/books/aerodynamics-for-engineering-students/houghton/978-0-08-049385-5

Hurt, H.H. (1965), *Aerodynamics for Naval Aviators*, Office of the Chief of Naval Operations, Aviation Training Division, available at: www.faa.gov/sites/faa.gov/files/regulations_policies/handbooks_manuals/aviation/00-80T-80.pdf

Kuethe, A. and Chow, C.-Y. (1997), *Foundations of Aerodynamics: Bases of Aerodynamic Design*, 5th ed., Wiley, available at: www.wiley.com/en-ie/Foundations+of+Aerodynamics%3A+Bases+of+Aerodynamic+Design%2C+5th+Edition-p-9780471129196

Li, J., Bouhlel, M.A. and Martins, J.R.R.A. (2019), "Data-based approach for fast airfoil analysis and optimization", *AIAA Journal*, Vol. 57 No. 2, pp. 581-596, doi: 10.2514/1.J057129.

Loftin, L.K. (1946), "Theoretical and experimental data for a number of NACA 6A-Series airfoil sections", No. NACA-RM-L6J01.

Masters, D.A., Taylor, N.J., Rendall, T., Allen, C.B. and Poole, D.J. (2015), "Review of aerofoil parameterisation methods for aerodynamic shape optimisation", 53rd AIAA Aerospace Sciences Meeting, American Institute of Aeronautics and Astronautics, doi: 10.2514/6.2015-0761.

Menter, F.R. (1992), "Improved two-equation k-omega turbulence models for aerodynamic flows", No. A-92183.

Moran, J. (2003), *An Introduction to Theoretical and Computational Aerodynamics*, John Wiley and Sons, New York, doi: 10.1017/S0001924000015001.

Nived, M.R., Mukesh, B.S., Athkuri, S.S.C. and Eswaran, V. (2021), "On the performance of RANS turbulence models in predicting static stall over airfoils at high Reynolds numbers", *International Journal of Numerical Methods for Heat and Fluid Flow*, Vol. 32 No. 4, pp. 1299-1323, doi: 10.1108/HFF-08-2021-0519.

Nonhoff, M. and Müller, M.A. (2022), "Online convex optimization for data-driven control of dynamical systems", *IEEE Open Journal of Control Systems*, Vol. 1, pp. 180-193, doi: 10.1109/OJCSYS.2022.3200021.

Rajnarayan, D., Ning, A. and Mehr, J.A. (2018), "Universal airfoil parametrization using B-Splines", 2018 Applied Aerodynamics Conference, American Institute of Aeronautics and Astronautics, doi: 10.2514/6.2018-3949.

Riegels, F.W. (1961), "Aerofoil sections: results from wind-tunnel investigations, theoretical foundations", Butterworths.

Shahrokhi, A. and Jahangirian, A. (2007), "Airfoil shape parameterization for optimum Navier–Stokes design with genetic algorithm", *Aerospace Science and Technology*, Vol. 11 No. 6, pp. 443-450, doi: 10.1016/j.ast.2007.04.004.

Siegler, J., Ren, J., Leifsson, L., Koziel, S. and Bekasiewicz, A. (2016), "Supersonic airfoil shape optimization by variable-fidelity models and manifold mapping", *Procedia Computer Science*, Vol. 80, pp. 1103-1113, doi: 10.1016/j.procs.2016.05.416.

Singh, S., Majumdar, A., Slotine, J.-J. and Pavone, M. (2017), "Robust online motion planning via contraction theory and convex optimization", 2017 IEEE International Conference on Robotics and Automation (ICRA), presented at the 2017 IEEE International Conference on Robotics and Automation (ICRA), pp. 5883-5890, doi: 10.1109/ICRA.2017.7989693.

Sobieczky, H. (1999), "Parametric airfoils and wings", in Fujii, K. and Dulikravich, G.S. (Eds), *Recent Development of Aerodynamic Design Methodologies: Inverse Design and Optimization*, Vieweg +Teubner Verlag, Wiesbaden, pp. 71-87, doi: 10.1007/978-3-322-89952-1_4.

Sturm, J.F. (1999), "Using SeDuMi 1.02, a Matlab toolbox for optimization over symmetric cones", *Optimization Methods and Software*, Vol. 11 Nos 1/4, pp. 625-653, doi: 10.1080/10556789908805766.

Tutuncu, R.H., Toh, K.C. and Todd, M.J. (2003), "SDPT3 — a Matlab software package for semidefinite-quadratic-linear programming, version 3.0".

Tyan, M., Park, J., Kim, S. and Lee, J. (2013), "Design optimization of subsonic airfoil and slotted flap shape using Multi-Fidelity aerodynamic analysis", 21st AIAA Computational Fluid Dynamics Conference, American Institute of Aeronautics and Astronautics, doi: 10.2514/6.2013-2704.

Vanderplaats, G. (1979), "An efficient algorithm for numerical airfoil optimization", 17th Aerospace Sciences Meeting, American Institute of Aeronautics and Astronautics, doi: 10.2514/6.1979-79.

Wilcox, D.C. (2006), *Turbulence Modeling for CFD* (Third Edition), DCW Industries, available at: www.amazon.com/Turbulence-Modeling-CFD-Third-Edition/dp/1928729088

Zhang, F., Chen, S. and Khalid, M. (2023), "Multi-Point optimization of transonic wing by real-coded genetic algorithm".

Zhu, Z., Schmerling, E. and Pavone, M. (2015), "A convex optimization approach to smooth trajectories for motion planning with car-like robots", arXiv, 26 October, doi: 10.48550/arXiv.1506.01085.

Corresponding author
Naef A.A. Qasem can be contacted at: naefqasem@kfupm.edu.sa